ROYAL SOCIETY
OF CHEMISTRY

PAPER

Check for updates

Alkali-activated materials from steel industry slags: optimization of prewashing and its effect on zinc adsorption and regeneration†

M. Korhonen, [ID] P. Dahl, T. Kangas, [ID] S. Tuomikoski, A. Heponiemi, [ID] T. Hu, [ID]
U. Lassi [ID] and H. Runtti*

Interest in alkali-activated materials (AAMs) has increased because of their effectiveness as adsorbents and their low cost. An additional advantage of AAMs is that raw materials obtained from industrial side streams can support a circular economy. In this study, slags from the steel industry were used as raw materials for an AAM. As the material was highly alkaline, prewashing was mandatory before adsorption studies to avoid precipitation of hydroxides. As washing agents, different concentrations of several chemicals (strong and weak acids) were used. Among them, oxalic acid performed the best by stabilizing the pH near neutral during adsorption and minimizing mass loss. Thus, using oxalic acid, prewashing was optimized in relation to the time and concentration. In adsorption experiments, the adsorption capacity was 78 mg g^{-1} for zinc, which was 18 times higher than that without optimization. The AAM adsorbent was also regenerable with oxalic acid because its adsorption efficiency remained stable in the next adsorption cycle. The AAM was characterized by X-ray diffraction (XRD), X-ray photoelectron spectroscopy (XPS), X-ray fluorescence (XRF), field emission scanning electron microscopy with energy dispersive X-ray spectrometry (FESEM-EDS), and diffuse reflectance infrared Fourier transform spectroscopy (DRIFTS). Analyses showed how prewashing affected the surface structure and functional groups in different process stages. The adsorption mechanism was determined to be complex formation. This study not only revealed more environmentally friendly options for material preparation but also showed how to improve environment quality with more advanced material preparation and process optimization methods.

1. Introduction

In the European Union, 25.5 million m^3 of industrial wastewater is produced each year, of which only 2.5% is reused.[1] There are many wastewater treatment methods. Among them, adsorption is an effective and a low-cost method for large volumes of water with low concentrations of heavy metals.[2,3] Key factors in the adsorption process are the pH, concentration, adsorbent dosage, and time.[4] Activated carbon, zeolites, geopolymers, and alkali-activated materials (AAMs) are the most common absorbents. Interest in developing adsorbents from side streams has increased. These adsorbents not only can be efficient but also can support a circular economy.[5]

The steel industry produces 190–290 million tons of steel slag as a side stream,[6] which is classified as a by-product.[7] Examples of steel slag are blast furnace slag (BFS) and ladle slag (LS). Steel slag has several properties suitable for an adsorbent raw material: high porosity, high specific surface area, and high density.[8] The use of slag in adsorbent applications is economically viable, as it is widely available, and its utilization does not produce secondary waste.[6] Slags that may require alkali activation are called AAMs and are considered as adsorbents. At present, AAMs are used to remove various impurities, such as heavy metals (*e.g.*, zinc), from wastewater.[9]

Zinc is a toxic pollutant, which enters the environmental system *via* industrial discharges and mining operations.[10,11] The amount of zinc in the industrial wastewaters depends on the operation, but usually the range is from a couple mg L^{-1} to 200 mg L^{-1} when adsorption is used.[12] Zinc is a potential risk for human health even at low concentrations, and for that reason it is crucial to remove it from aquatic systems to promote cleaner ecosystems.[13] One challenge in zinc removal is that zinc may act differently when competing metal cations and other interfering ions are available.[11] Industrial scale wastewater matrix is usually quite complex. However, in this study, zinc was investigated individually to obtain trustworthy data from experimental design tools. Another challenge is that alkali activation makes the AAMs highly alkaline, which causes the precipitation of metal ions as hydroxides. For example, zinc precipitation occurs at pH 8.[14] Accordingly, AAMs must be neutralized after

Research Unit of Sustainable Chemistry, University of Oulu, P.O. Box: 4300, FI-90014, Oulu, Finland. E-mail: hanna.runtti@oulu.fi

production by environmentally friendly preliminary washing (prewashing) prior to their use in water treatment.

To effectively study the adsorption conditions and mechanism, it is important to use prewashing of the AAM to ensure that the contaminant is adsorbed. Only a few publications in the literature have examined prewashing of the material. In terms of prewashing agents, acetic acid,[15,16] nitric acid,[17] hydrochloric acid,[18,19] or water has only been used to obtain neutral materials.[20–22] Using the latter agent, a lot of water is consumed. The other agents affect the structure of the AAM by breaking its bonds.[23] Thus, prewashing has a significant effect on the material's adsorption properties, and it may have negative environmental impacts as such. Information on prewashing and its effects on the AAMs is incomplete. By filling the gap in the current knowledge, not only water consumption in material preparation can be decreased but also greener options for pretreatment can be applied to improve global environmental management and efforts in sustainability.

The aim of this study was to investigate the effect of different prewashing agents on the use of an AAM as an adsorbent to offer more environmentally viable methods. The AAM was prepared from an industrial side stream slag (BFS and LS). It was used to adsorb zinc in batch mode adsorption experiments to examine its adsorption efficiency. This study focused on different prewashing chemicals (nitric acid, hydrochloric acid, acetic acid, and oxalic acid). To the best of our knowledge, oxalic acid has not previously been used as a prewashing agent. Comparison of prewashing agents was done by evaluating material loss and the pH change during the prewashing process. In zinc adsorption experiments, the most promising prewashing chemical (i.e., oxalic acid) was then optimized in terms of washing time and concentration. The aim was to achieve the highest adsorption capacity (q-value). A face-centered central composite design (CCF) was selected as a model for the optimization studies using the selected prewashing agent. Regeneration was studied using oxalic acid at concentrations of 0.05–0.2 M (pH of approximately 6). The efficiency was estimated based on the adsorption efficiency achieved after regeneration. Finally, the AAM was studied by X-ray diffraction (XRD), X-ray fluorescence (XRF), X-ray photoelectron spectroscopy (XPS), field emission scanning electron microscopy with energy dispersive X-ray spectrometry (FESEM-EDS), and diffuse reflectance infrared Fourier transform spectroscopy (DRIFTS). The adsorption mechanism of the AAM is discussed based on the results of this study.

2. Materials and methods

2.1. Chemicals

In this study, BFS and LS were used as raw materials for adsorbent preparation. Both slags were obtained from a European steel producer. Elemental analysis of both slags is presented in an earlier study.[21] For adsorbent preparation, sodium hydroxide (NaOH) (VWR Chemicals, Belgium) and sodium silicate (Na_2SiO_3) (VWR International, USA) were used in the alkali-activation process. An adsorbate solution was prepared from zinc chloride salt ($ZnCl_2$) (VWR Chemicals, Belgium).

For prewashing and regeneration, nitric acid (HNO_3) (Thermo Fisher Scientific, Germany), hydrochloric acid (HCl) (FF Chemicals), acetic acid (CH_3COOH) (VWR Chemicals, Belgium), and oxalic acid dihydrate ($(COOH)_2 \cdot 2H_2O$) (VWR Chemicals, Belgium) were used. For pH adjustment, NaOH (VWR Chemicals, Belgium) was used.

2.2. Preparation of the adsorbent

The adsorbent material was prepared from BFS and LS via the alkali-activation process, using a method from previous studies with modification.[16,21] The preparation procedure is presented in Fig. 1. Before alkali activation, the LS slag was sieved to particle size below 0.125 mm and then mixed with the BFS slag (w/w 1 : 1). For alkali activation, the alkaline solution was prepared by mixing 10 M NaOH and Na_2SiO_3 solutions (w/w 1 : 1). The alkaline solution was stirred using a homogenizer (Velp Scientifica OV5 Homogenizer, Italy), and the BFS/LS mix was slowly added (w/w 2 : 3). After addition, stirring was continued for 10 minutes at full speed (1250 rpm). The material was then added into silicone molds and kept at 25 °C for one week for hardening.

The AAM was first crushed using a jaw crusher (Jaw Crusher, BB51) and then sieved to particle size below 4 mm. After precrushing, the AAM was crushed using a rod mill (Rod Mill, Wedag) to 0.125–0.5 mm particle size. The AAM was then dried in an oven at 105 °C for 48 hours.
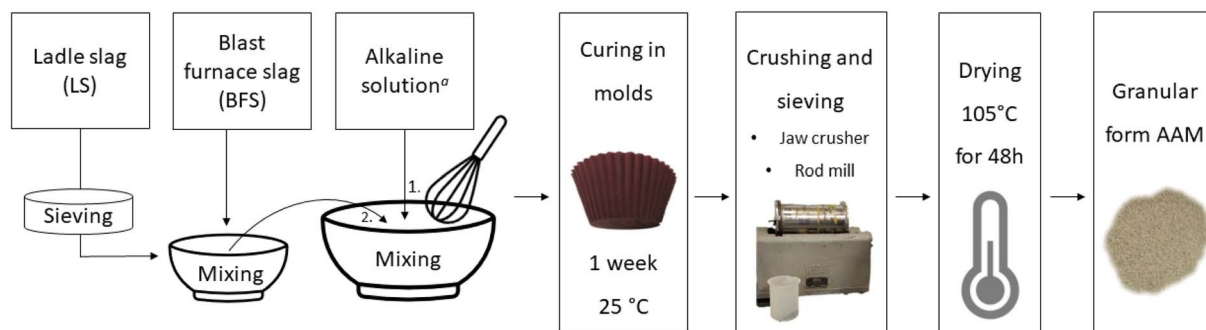

Fig. 1 Preparation of the AAM.

This journal is © The Royal Society of Chemistry 2025

J. Mater. Chem. A, 2025, **13**, 20984–20997 | **20985**

2.3. Characterization of the material

To shed light on the adsorption mechanism and functionality changes during processing, the adsorbent material was characterized by XRD, XRF, XPS, FESEM-EDS, and DRIFTS. All samples were analyzed before oxalic acid prewashing and also before and after adsorption.

The XRD patterns were recorded with a PANalytical X'Pert Pro X-ray diffractometer (Malvern Panalytical, Almelo, The Netherlands) using monochromatic Cu Kα_1 radiation (λ = 1.5406 Å) at 45 kV and 40 mA. Diffractograms were collected over the 2θ range of 6–90° at 0.017° intervals and with a scan step time of 60 seconds. The crystalline phases and structures were analyzed using HighScore Plus software. The XRF results were measured with a PANalytical Axios mAX 4 kW Wavelength Dispersive X-ray fluorescence spectrometer (Malvern Panalytical, Almelo, The Netherlands). The measurements were done using loose powders through a Mylar film in a He atmosphere. Elemental mapping and composition analysis were carried out by FESEM-EDS using a Zeiss Ultra Plus (Carl Zeiss Microscopy GmbH, Jena, Germany) with AZtec software (Oxford Instruments) at the Centre for Material Analysis in the University of Oulu, Finland. The instrument was operated at 15 kV and a working distance of 8.5 mm. XPS analysis was performed at the Centre for Material Analysis, University of Oulu, Finland, using an ESCALAB 250Xi XPS System (Thermo Fisher Scientific, Waltham, MA, USA). The samples were placed on a gold sample holder. A high-resolution scan was then conducted using a pass energy of 20 eV, and a survey scan was conducted using a pass energy of 150 eV. The monochromatic Al Kα radiation (1486.7 eV) source was operated at 20 mA and 15 kV with an X-ray spot size of 900 μm. The concentrations of oxygen, calcium, silica, magnesium, and carbon were measured for all samples, and the measured data were analyzed using the Avantage V5 program. Charge compensation was performed by applying the C 1s line at 284.8 eV as a reference. DRIFTS was used to analyze the degree of polymerization and the effect of oxalic acid on the structure of the prepared AAM. A Bruker PMA 50 Vertex 80 V (Bruker, Billerica, MA, USA) equipped with a Harrick Praying Mantis diffuse reflection accessory and a high-temperature reaction chamber was utilized to scan the DRIFT spectra at 400–4000 cm^{-1} with a resolution of 4 cm^{-1} and 500 scans per minute. The baseline was measured using potassium bromide.

2.4. Prewashing of the material

For prewashing, different acids (nitric acid, hydrochloric acid, acetic acid, and oxalic acid) were used. Prewashing took place at 25 °C, and the reaction time was 24 h. Mass loss and pH change served as indicators of the suitability of different prewashing agents. The most promising prewashing agent was then optimized in terms of the prewashing time and acid concentration.

2.4.1. Strong acids.
Nitric acid and hydrochloric acid with concentrations of 0.01 M and 0.05 M, respectively, were studied for prewashing in batch mode. The AAM was weighed and placed in a beaker, and the prewashing chemical was added in a ratio of 5.8 g L^{-1}. The mixture was stirred with a magnetic stirrer at 300 rpm for 24 hours, and the AAM was then rinsed with water until the pH was stable.

2.4.2. Acetic acid.
Experiments with different concentrations of acetic acid (0.01 M, 0.05 M, and 0.1 M) as a prewashing chemical were conducted as described in Section 2.4.1.

2.4.3. Oxalic acid.
Oxalic acid was studied with different prewashing times (2, 4, 6, 18, and 24 h) and concentrations (0.05 M, 0.07 M, 0.1 M, 0.2 M, 0.3 M, 0.4 M, and 0.5 M). Batch experiments were done by adding 0.2 g of AAM and 35 ml of oxalic acid to a 50 ml Falcon tube. The Falcon tube was then placed in a shaker at 300 rpm for the selected time. The mass loss and pH were then measured, followed by adsorption experiments.

2.5. Adsorption experiments

Adsorption was studied at different levels. First, the optimization of prewashing time and concentration of prewashing agent was investigated. How the prewashing affect the AAMs' ability to adsorb was studied. After that, adsorption conditions were optimized by using an experimental design tool. All the samples from the adsorption tests were preserved with strong nitric acid and analyzed by flame atomic absorption spectroscopy (Varian AA240FS; Varian Inc. Palo Alto, CA, USA).

2.5.1. The effect of oxalic acid prewashing concentration on adsorption.
Adsorption experiments of the prewashed AAMs were conducted as described in Section 2.4.3. Zinc was used as an adsorbate to be attached to the AAM. The concentration of zinc was 80 mg L^{-1}. All adsorption tests were done in 50 ml Falcon tubes. The adsorbent/adsorbate ratio (5 g L^{-1}), agitation rate (300 rpm), and adsorption time (24 hours) were kept constant at 25 °C. The pH was measured at the beginning of the experiment and at the end of the experiment to ensure that zinc removal was not caused by precipitation.

2.5.2. Optimizing the adsorption conditions by using an experimental design.
The adsorption experiments were optimized in batch mode, keeping the adsorbate solution volume (0.15 L) and adsorption time (24 hours) constant. A face-centered central composite design (CCF) was selected as a model for optimization studies. The run order was randomized, and the model included 14 runs and three center points. Adsorption efficiency (q_e) and removal percentage (R-%) were selected as the main responses, which were determined using eqn (1) and (2), respectively.

$$q = \left(\frac{c_0 - c}{m}\right) \times V \tag{1}$$

$$R\text{-}\% = \frac{c_0 - c}{c_0} \times 100\% \tag{2}$$

where c_0 is the initial concentration (mg L^{-1}), c is the concentration after adsorption (mg L^{-1}), m is the adsorbent mass (g), and V is the volume of the adsorbate solution (L).[24,25]

MODDE Pro 13 software was used for the experimental design setup and analysis. Table 1 shows the variables included in the optimization experiments.

20986 | J. Mater. Chem. A, 2025, 13, 20984–20997

This journal is © The Royal Society of Chemistry 2025

Table 1 Factors input for adsorption optimization in the CCF

Factor	Low	High
Concentration (mg L^{-1})	100	500
Dosage (g L^{-1})	2	10
Initial pH	4	6

2.6. Regeneration

To determine the regenerative potential of the AAM, it was first prewashed with 0.05 M oxalic acid. Prewashing was done in batch mode in a Flocculator 2000 (Kemira AB, Sweden) to prevent mechanical grinding. Batch adsorption experiments were then done using zinc solution (100 mg L^{-1}) for the prewashed AAMs. Regeneration experiments were conducted in 50 ml Falcon tubes. In the regeneration experiments, 0.4 g of zinc-adsorbed AAM and 20 ml of regeneration solution (oxalic acid at concentrations of 0.05 M, 0.1 M, and 0.2 M) were combined. They were placed in a shaker at 300 rpm for different times (10, 30, 60, 120, and 240 minutes). The pH was adjusted in the beginning to 6 with NaOH. Further adsorption batch experiments were conducted by using the regenerated AAM. The impact of the regeneration chemical's (oxalic acid) concentration and regeneration time on the efficiency of the next adsorption cycle was investigated. Regeneration efficiency was calculated as presented in eqn (3).

$$R\text{-}\% = \left(\frac{q_n}{q_1}\right) \times 100\% \tag{3}$$

where q_1 is the initial adsorbed amount (mg g^{-1}) and q_n is the adsorbed amount after the nth cycle (mg g^{-1}).[26]

3. Results and discussion

3.1. Characterization of the AAM

To shed light on the adsorption mechanism, different characterization analyses were done on the AAM. The AAM was characterized before and after prewashing and also after adsorption of zinc. The aim of this study was to reveal what is removed from the AAM during washing and how the zinc is adsorbed to the AAM.
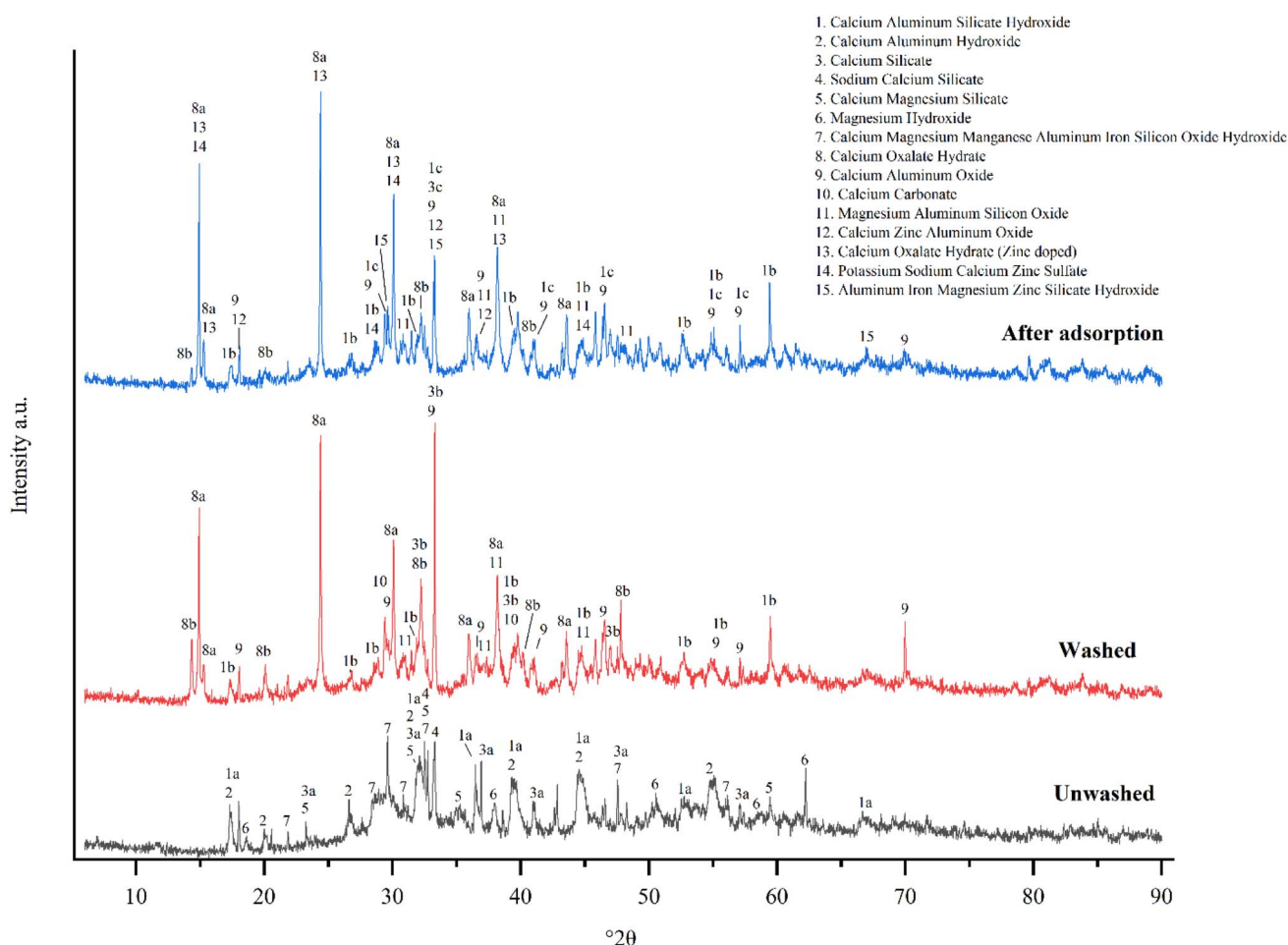

Fig. 2 Results of XRD analysis of the unwashed, oxalic acid-washed, and zinc-adsorbed AAM (a–c are the same compound with different reference numbers).

This journal is © The Royal Society of Chemistry 2025

J. Mater. Chem. A, 2025, **13**, 20984–20997 | **20987**

Table 2 XRF analysis of the unwashed, oxalic acid-washed, and zinc-adsorbed AAM

Metal oxide	CO$_2$	SO$_3$	H$_2$O	Na$_2$O	MgO	Al$_2$O$_3$	SiO$_2$	P$_2$O$_5$	K$_2$O	CaO	TiO$_2$	MnO	Fe$_2$O$_3$	ZnO
Unwashed	6.5	1.8	34.8	8.2	3.2	6.8	15.5	0.6	0.2	20.9	0.6	0.3	0.4	0.0
Washed	14.9	0.9	56.4	0.0	0.3	2.4	7.1	0.4	0.0	16.6	0.4	0.1	0.3	0.0
Zinc adsorbed	12.6	0.8	55.6	0.0	0.4	3.4	8.6	0.5	0.0	15.8	0.5	0.2	0.3	1.3

3.1.1. X-ray diffraction. The XRD results are presented in Fig. 2. More detailed information on the reference data of the XRD can be found in the ESI.† The results showed that pre-washing with oxalic acid affected calcium-containing groups on the surface of AAM. It was also seen that calcium oxalate hydrate formed. In addition, the calcium aluminum hydroxide content decreased in relation to calcium aluminum oxide. Based on the XRD results, oxalic acid washing oxidized the surface of the AAM. A small amount of calcium magnesium manganese aluminum iron silicon oxide hydroxide was present in the material before washing. After washing, magnesium, manganese, and iron were removed from this specific phase where it was attached. As calcium had strong bonds with aluminum and silica in the material, it was not removed. Comparison of the prewashed material and the material after zinc adsorption revealed that zinc was attached to calcium aluminum oxide. In addition, zinc was also attached to calcium oxalate hydrate on the surface. XRD analysis revealed that zinc doped calcium oxalate hydrate overlapped with the calcium oxalate hydrate peak at 14.9°. The formation of calcium oxalate hydrate on the surface of AAM affected the adsorption mechanism of zinc.

3.1.2. X-ray fluorescence. To reveal the metal oxide content and how it changed during washing and adsorption, XRF analysis was conducted. The XRF results are presented in Table 2. Washing affected both the carbon dioxide and water contents due to the attachment of oxalic acid hydrate to the calcium-containing groups on the surface of AAM. In addition, washing led to a decrease in the aluminum oxide, magnesium

oxide, silicate, sodium oxide, and calcium oxide contents, which resulted in mass loss of the AAM.

3.1.3. X-ray spectroscopy. To shed light on elemental bonding in the material, XPS analysis was conducted. The results of XPS analysis and O 1s transformation are presented in Fig. 3 and 4, respectively. The analysis showed that sodium and magnesium were washed away from the surface (Fig. 3). Of note, XPS analysis revealed that the oxygen in the metal carbonate form was transformed to an oxide form during prewashing. This can be seen by comparing the unwashed (a) and washed (b) AAM (Fig. 4). Also, XRF results support these observations. In addition, the number of C–O–H groups and C=O groups decreased during adsorption. Due to that, a slight increase in the C–O peak can be seen when the washed (b) and zinc-adsorbed (c) AAMs are compared (Fig. 4). Based on these results, it can be concluded that zinc cations most probably doped with calcium oxalate, which was also supported by the XRD results.

3.1.4. Field emission scanning electron microscopy with energy dispersive X-ray spectrometry. The surface of the AAM was also characterized by FESEM-EDS. The images are presented in Fig. 5, and the content table of elements on the surface is presented in Table 3. The analyses revealed small crystallite formation during the washing process. Elemental changes on the surface of the AAM were detected using EDS. Washing increased the amount of oxygen and carbon although copper, potassium, titanium, and iron were washed away from the surface of the AAM. In addition, manganese was removed from the AAM by washing, and zinc was attached to the place of magnesium during adsorption. The results indicated that zinc ions are more likely to attach to surface sites occupied by aluminum, sodium, and silica. However, as can be seen in Fig. 5(c and d), zinc is clearly attached to the same sites as magnesium. Thus, zinc competes with magnesium for adsorption sites.

3.1.5. Diffuse reflectance infrared Fourier transform spectroscopy. DRIFT spectra of unwashed and oxalic acid washed AAM as well as AAM after zinc adsorption are described in Fig. 6. The unwashed sample presented several peaks related to the formation of Si–O–Si and Al–O–Si during preparation of the material. The peak at around 3660 cm^{-1} was attributed to the hydrogen-bonded silanol (vicinal or geminal silanol groups[27]), while the broad peak at around 3480 cm^{-1} and another peak at 1640 cm^{-1} were assigned to the absorbed molecular water in the sample.[28] The peaks observed at around 1535 cm^{-1} and 1380 cm^{-1} were attributed to the CO$_3^{2-}$ asymmetric stretching.[29] The typical Si–O–Si and Al–O–Si strong asymmetric stretching were present in the 950–1250 cm^{-1} (ref. 30)
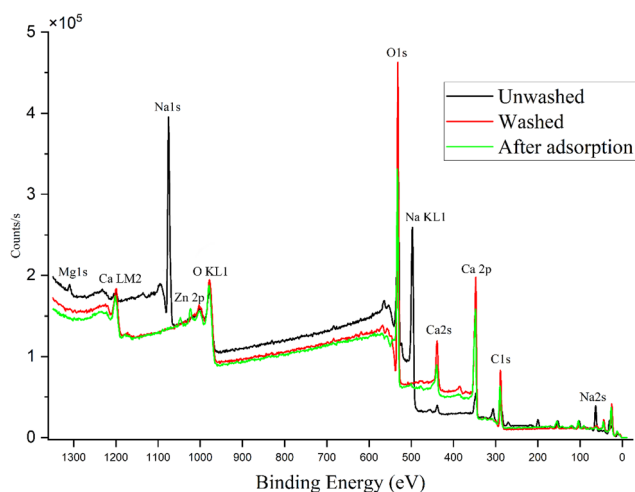

Fig. 3 Results of XPS analysis of the unwashed, oxalic acid-washed, and zinc-adsorbed AAM.
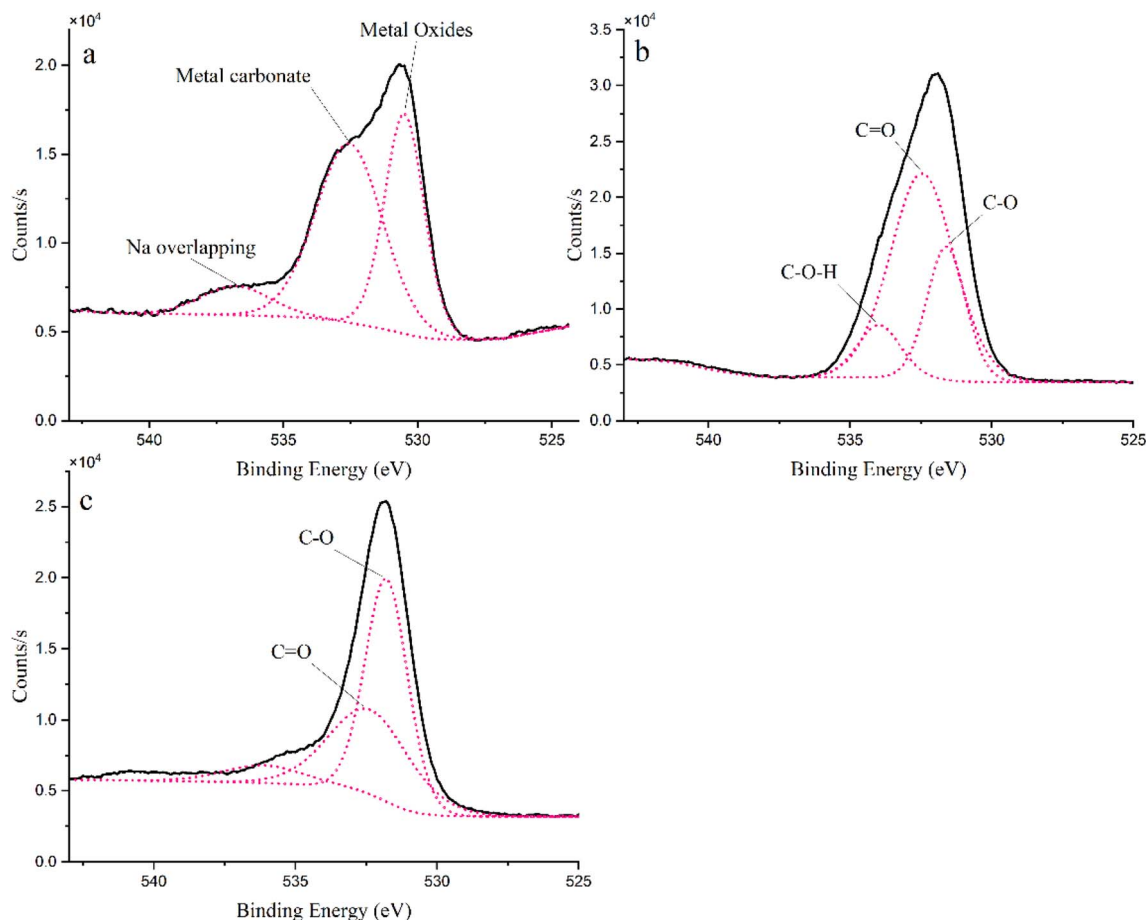
Fig. 4 Results of XPS (O 1s) analysis of the (a) unwashed, (b) oxalic acid-washed, and (c) zinc-adsorbed AAM. Note that the X-axis does not start from zero.

wavenumber region with the peak center at around 1120 cm^{-1} in the unwashed sample. Moreover, the broad peak with a center at around 730 cm^{-1} was related to the Si–O–Si and Al–O–Si symmetric stretching.[31] After oxalic acid washing, the change in the surface structure before and after zinc adsorption was obvious compared to the unwashed sample. Both samples presented several peaks related to oxalic acid treatment. The peaks at around 3500 cm^{-1} and 3080–3095 cm^{-1} were attributed to the OH stretching and H-bonded OH stretching of carboxylic acids,[31] respectively. Moreover, the very strong peak at around 1723 cm^{-1} was assigned to C=O stretching in carbonyl compounds, while another strong peak at around 1350 cm^{-1} was attributed to C=O stretching of carboxylic acids.[32] In addition, peaks at around 615 cm^{-1} and 484 cm^{-1} were assigned to O–C=O bending and C–C=O bending in carboxylic acids,[31] respectively. However, the broad peak at around 730 cm^{-1} observed for the unwashed sample was split in the DRIFT spectra of oxalic acid washed sample and sample after zinc adsorption, revealing that after oxalic acid washing part of the amorphous structure of the AAM has disappeared. This can also be observed from the X-ray diffractograms of the oxalic acid washed sample and sample after adsorption (Fig. 2)

in which the amorphous "hump" in the 2θ range of approximately 27–29° is missing.[33,34]

3.1.6. Adsorption mechanism. In general, adsorption mechanisms can be divided into two main categories: physisorption and chemisorption. In physisorption, bonds between the adsorbate and adsorbent are weak compared to chemisorption. Both physisorption and chemisorption can be divided into subcategories. For physisorption, these subcategories are attractive electrostatic forces, van der Waals forces, hydrophobic interactions and hydrogen bonding. Chemisorption can be divided into ion-exchange, precipitation, complex formation and chemical reduction.[35–37] In this study, the adsorption mechanism was investigated by several characterization methods to reveal how zinc is adsorbed to the AAM.

XRD and DRIFTS results (Fig. 2 and 6) indicated that, while prewashing, the anionic oxalate was bound to the calcium on the AAM surface. This finding was also supported by FESEM-EDS (Fig. 5), which indicated that due to washing, the amount of carbon and oxygen increased. XRD results also showed that after adsorption, calcium oxalate doped with zinc. XPS results (Fig. 4) showed similar findings. This revealed that zinc was adsorbed directly onto the carboxylic group on the surface, as
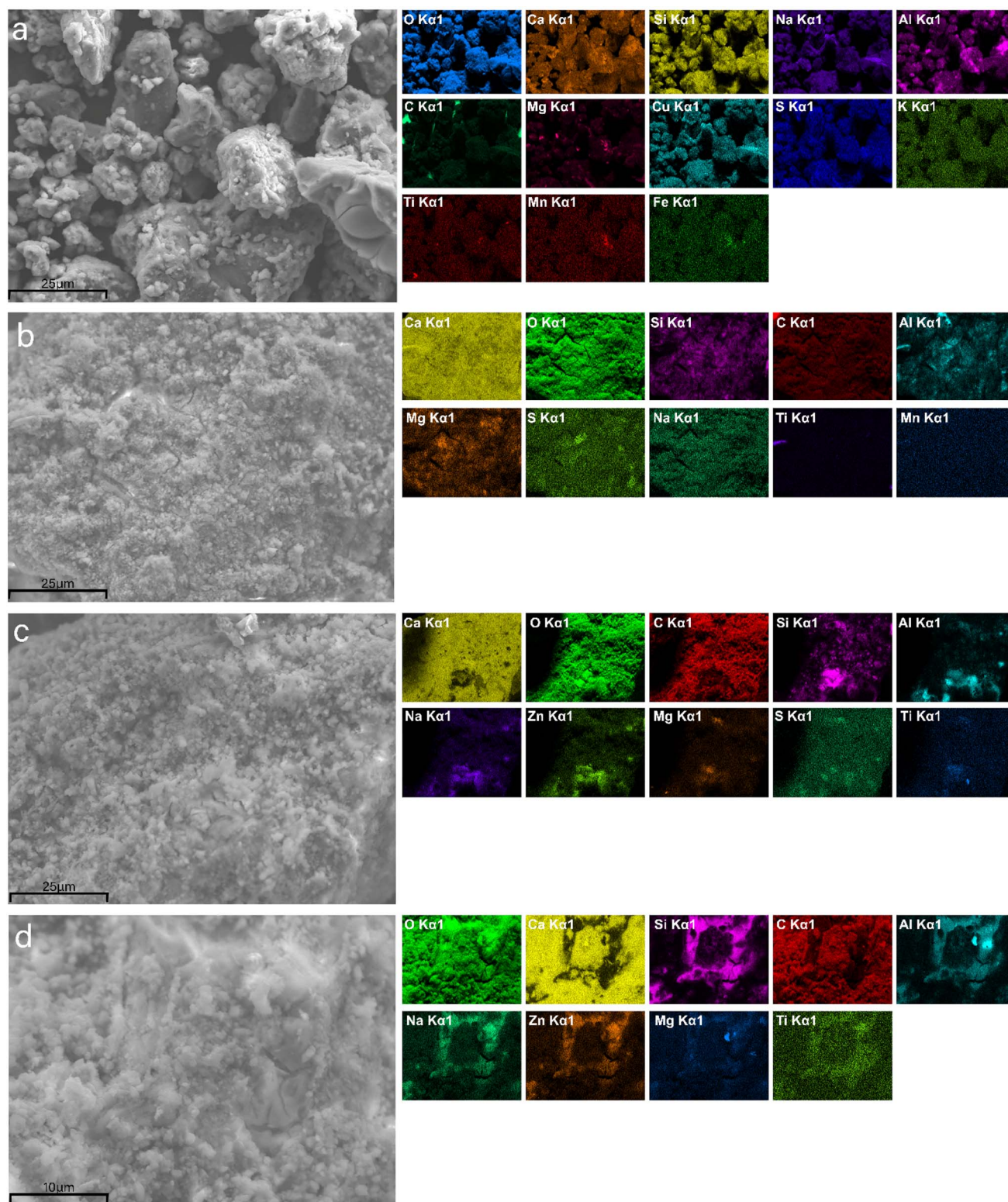
Fig. 5 FESEM-EDS images of (a) unwashed (25 μm), (b) oxalic acid-washed (25 μm) and (c and d) zinc-adsorbed (25 μm and 10 μm, respectively) AAM.

illustrated in Fig. 7. Because of this, the hydroxyl groups transformed into C–O groups.[38] Therefore, in the XPS results (Fig. 4b), the ratio of C–O groups increased when compared to the number of C=O groups. In other words, the amount of C=O groups remained the same, even though the ratio of C–O and C=O groups changed. In summary, these results indicated

20990 | J. Mater. Chem. A, 2025, 13, 20984–20997

This journal is © The Royal Society of Chemistry 2025

Table 3 Map sum spectrum of unwashed, oxalic acid-washed, and zinc-adsorbed AAM from FESEM-EDS measurements

Element	Weight%		
	Unwashed	Washed	Zinc adsorbed
O	47.7	58.5	57.6
Ca	19.3	30.4	32.1
Na	11	0.2	0.2
Si	10.8	6.2	5
Al	5	3	2.8
Mg	2.9	0.7	0.3
Cu	1.6	0	0
Ti	0.5	0.3	0.3
S	0.5	0.4	0.1
Mn	0.3	0.2	0
K	0.3	0	0
Fe	0.3	0	0
Zn	0	0	1.5
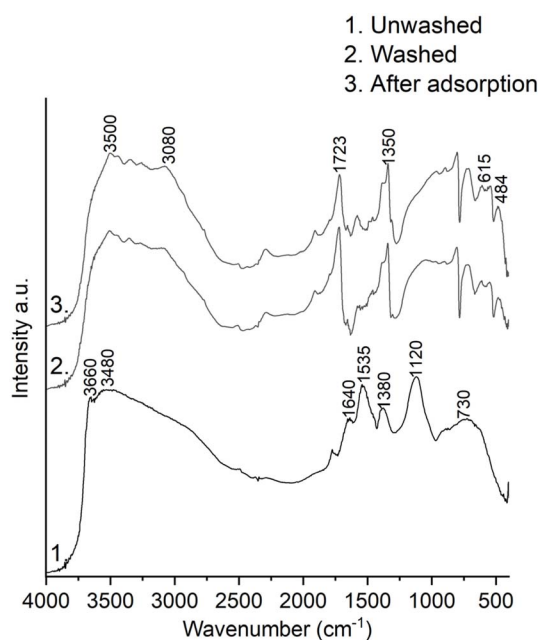
Fig. 6 DRIFT spectra of the unwashed, oxalic acid-washed and zinc-adsorbed AAM.

that zinc cations are adsorbed to the AAM with the mechanism of complex formation.[38] A simplified mechanism of complex formation is presented in Fig. 7.

3.2. Prewashing

The AAM was prewashed with different chemicals to achieve the highest adsorption capacity and endurance in the adsorption process. Without prewashing, the adsorption experiment's pH would increase over the limit value (pH 8). A too high pH value would cause zinc precipitation as hydroxide. To avoid precipitation, a large variety of different acids were studied for prewashing and compared.

3.2.1. Strong acids. Table 4 presents the results of prewashing of the AAM with hydrochloric and nitric acid at concentrations of 0.01 M and 0.05 M. The results showed that these strong acids destroyed the AAM due to mass loss, as reported in the literature.[39] Prewashing with these strong acids was not effective enough to stabilize the pH. In addition, when the material was prewashed with nitric acid (0.05 M), material loss was high (60–100%). Material loss was assumed to be due to a neutralization reaction between the AAM and the acid, which negatively affected the material's mechanical strength. Thus, in subsequent experiments, the AAM was prewashed with weak acids.

3.2.2. Acetic acid. In this study, acetic acid as a prewashing chemical was evaluated at concentrations of 0.01 M, 0.05 M, and 0.1 M. Weak acids are more effective than strong acids in prewashing of AAMs. The concentration of the weak acid is also crucial. In this study, 0.05 M acetic acid was considered the most effective prewashing agent based on the stabilized pH value. However, material loss of the AAM was still high (Table 5). With lower acetic acid concentrations, prewashing did not stabilize the pH to a neutral level. On the other hand, higher concentrations of acetic acid destroyed the material. Therefore, in subsequent experiments, oxalic acid was used as a prewashing agent.

3.2.3. Oxalic acid. Prewashing with oxalic acid was studied in batch experiments. Table 6 presents the results obtained using different oxalic acid concentrations (0.05–0.5 M) and washing times (2–24 hours). At an oxalic acid concentration of 0.05 M, the minimum washing time required to achieve favorable pH value and stability was 18 hours. However, when the
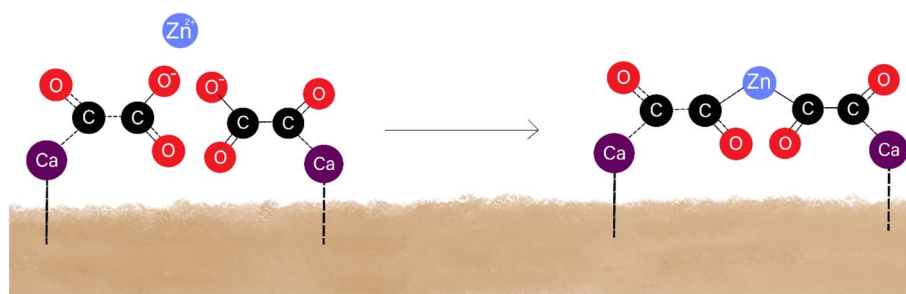

Fig. 7 Simplified mechanism of complex formation.

This journal is © The Royal Society of Chemistry 2025

J. Mater. Chem. A, 2025, **13**, 20984–20997 | **20991**

Table 4 Strong acids: mass loss during prewashing and the pH after rinsing with deionized water

Chemical	Concentration (M)	Washing time (h)	Stabilized pH	Mass loss (%)
Hydrochloric acid	0.01	24	9.83	73.1
Hydrochloric acid	0.05	24	9.01	100
Nitric acid	0.01	24	10.19	33.1
Nitric acid	0.05	24	9.22	60.9

Table 5 Acetic acid: mass loss during washing and the pH after rinsing with deionized water

Chemical	Concentration (M)	Washing time (h)	Stabilized pH	Mass loss (%)
Acetic acid	0.01	24	10.17	22.4
Acetic acid	0.05	24	6.37	72.5
Acetic acid	0.1	24	6.12	100

concentration was increased to 0.5 M, a washing time of 2 hours was sufficient to stabilize the pH to a neutral value. However, at a concentration of 0.05 M, mass loss was slightly lower. In addition, the particle size remained unchanged with 0.05 M oxalic acid compared to those which were prewashed with higher concentrations. Mass loss in oxalic acid prewashing was lower despite the concentration. Also, the pH value was more stable and mass loss was lower when compared to other pre-washing chemicals. Mass loss varied between 4.98% and 28.2% (Fig. 7) with oxalic acid. As shown in Fig. 8, neither the concentration nor time affected the mass loss linearly. Although the concentration and time affected the stabilized pH value linearly. Taken together, the results indicated that a combination of 0.05 M oxalic acid and a prewashing time of 18 hours were optimum to minimize mass loss and maintain pH stability.

Fig. 9 shows changes in color and form in the AAM after oxalic acid and acetic acid prewashing. The material washed with oxalic acid (b) was most similar in terms of form to the unwashed material (a), although the color of the oxalic acid washed material was lighter. Oxidation of the surface might have caused the change in color. Prewashing with acetic acid (c) led to a decrease in particle size and AAM breakdown.
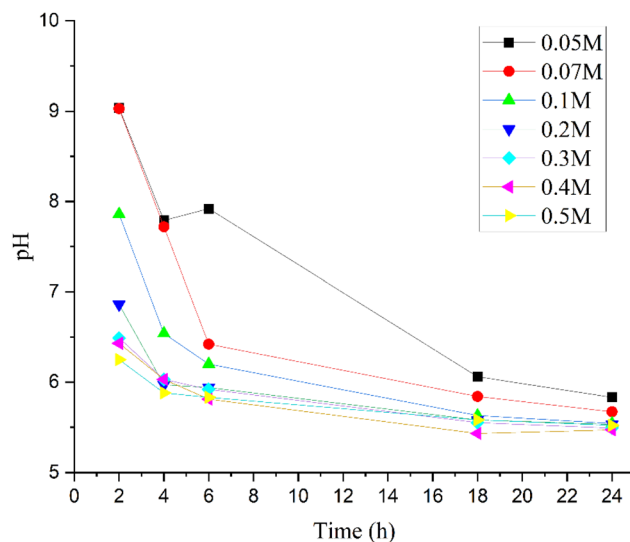
Fig. 8 Effect of oxalic acid concentration and time on pH stability. Note that the Y-axis does not start from zero. The liquid to solid ratio was 5g L^{-1} and temperature was 25 °C.

3.3. Adsorption experiments

The AAM showed high adsorption efficiency for zinc. Selecting the optimum prewashing chemical, concentration, and pre-washing time had a significant impact on its adsorption efficiency. In the literature, there is only a limited amount of information on prewashing highly alkaline AAMs. Usually, pure water is used for prewashing. No studies have focused on the washing time and the amount of water usage.

3.3.1. Prewashing with oxalic acid: the effect of oxalic acid concentration on adsorption. Prewashed AAMs were used in adsorption experiments to ensure that the pH did not rise above

Table 6 Stabilized pH and mass loss after oxalic acid washing

| Washing time	2 h		4 h		6 h		18 h		24 h	
Concentration (M)	pH_{end}	Mass loss (%)	pH_{end}	Mass loss (%)	pH_{end}	Mass loss (%)	pH_{end}	Mass loss (%)	pH_{end}	Mass loss (%)
0.05	9.04	20.05	7.79	20.84	7.92	22.46	6.06	21.61	5.83	12.40
0.07	9.03	21.02	7.72	20.05	6.42	20.00	5.84	16.35	5.67	13.05
0.1	7.86	19.82	6.54	21.84	6.20	20.39	5.63	16.99	5.54	4.98
0.2	6.86	19.64	5.97	15.52	5.94	10.58	5.58	16.3	5.53	15.99
0.3	6.49	17.60	6.03	16.88	5.92	17.85	5.55	16.01	5.49	12.33
0.4	6.43	18.46	6.03	17.45	5.81	15.55	5.43	12.25	5.47	16.63
0.5	6.25	28.21	5.88	23.02	5.83	17.14	5.58	23.37	5.52	20.37
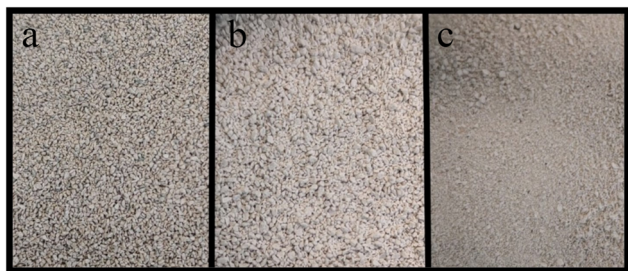
Fig. 9 The AAM (a) before prewashing, (b) 18 hours after prewashing with 0.05 M oxalic acid, and (c) 24 hours after prewashing with 0.05 M acetic acid.

8. The adsorption efficiencies and pH values after adsorption are presented in Table 7. By lowering the prewashing chemical concentration and increasing the prewashing time, the adsorption capacity was increased almost 18 times. This result is notable because in a previous study the authors reported that slag-based adsorbents did adsorb effectively metal cations, although oxalate ions were present in adsorption.[24]

3.3.2. Optimizing the adsorption conditions in an experimental design. The adsorption conditions were optimized in batch mode using a CCF design plan. This design had 14 runs and three center points. Two runs were excluded as outliers. The design matrix and responses are included in the ESI.† Based on

Table 7 The effect of the selected prewashing concentration and time on the adsorption capacity and pH at the end of adsorption

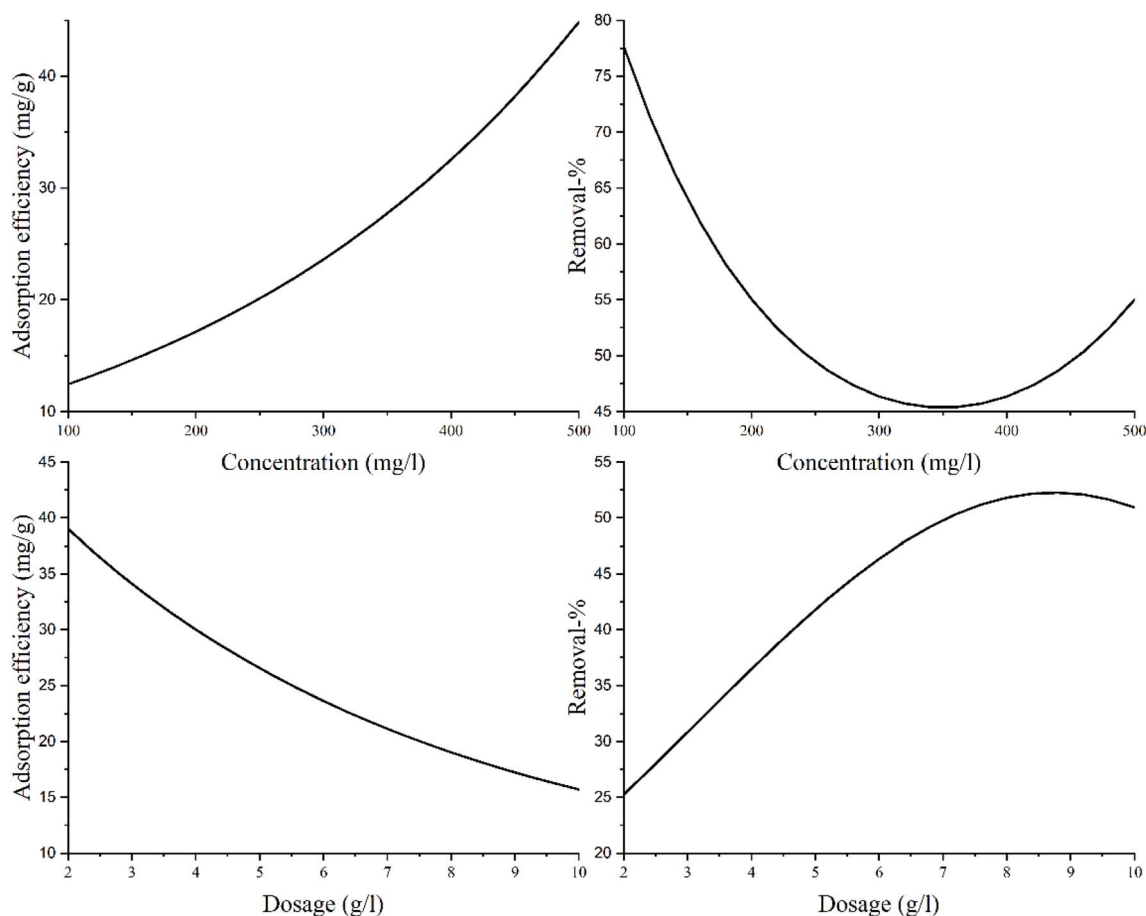| Washing time	2 h		4 h		6 h		18 h		24 h	
Concentration (M)	pH_{end}	q_e (mg g^{-1})	pH_{end}	q_e (mg g^{-1})	pH_{end}	q_e (mg g^{-1})	pH_{end}	q_e (mg g^{-1})	pH_{end}	q_e (mg g^{-1})
0.05							6.67	14.28	6.94	12.31
0.07							6.95	12.20	6.59	10.52
0.1					7.38	14.09	6.67	10.03	6.23	8.05
0.2			7.11	12.88	6.94	11.31	6.27	5.96	5.76	4.03
0.3			6.86	11.00	6.95	10.87	5.91	4.52	5.65	3.00
0.4	7.21	13.31	6.96	11.24	6.81	9.16	5.65	3.18	5.35	1.47
0.5	6.16	12.95	6.37	8.02	6.59	7.37	5.25	2.18	5.13	0.80

Fig. 10 Effect of concentration and adsorbent dosage on the adsorption efficiency and removal percentage using the CCF experimental design. The temperature was kept constant at 25 °C and adsorption time was 24 h. Note that the axes do not start from zero.

This journal is © The Royal Society of Chemistry 2025

J. Mater. Chem. A, 2025, 13, 20984–20997 | 20993

Table 8 AAM zinc adsorption capacity in the experimental study

AAM raw material	q (mg g^{-1})	Type	Ref.
BFS/LS	2.92	Column	21
Natural volcanic tuff	14.7	Batch	40
BFS/LS	17.27	Column	16
Metakaolin/fly ash	23.3	Batch	41
Metakaolin	35.88	Batch	42
Fly ash	47.1	Batch	43
Fly ash/chitosan	49–50	Batch	44
Fly ash	66.67	Batch	45
Metakaolin	74.53	Batch	25
BFS/LS	78.96	Batch	This study

the results, pH did not significantly affect the adsorption efficiency or removal percentage. The concentration of zinc was found to be the most important factor affecting the adsorption efficiency. By increasing the concentration, the removal percentage decreased, although the q-value increased. The opposite trend was seen when considering the effect of adsorbent dosage on the adsorption efficiency and removal percentage, as shown in Fig. 10.

The optimal conditions for zinc adsorption by the AAM were as follows: concentration of zinc of 500 mg L^{-1}, adsorbent dosage of 2 g L^{-1}, and pH of 5.9. A high adsorption capacity (78 mg g^{-1}) was achieved experimentally in this study. The capacity achieved was better than that reported in similar studies on AAM-based materials (Table 8).

3.4. Regeneration of the used AAM

After the adsorption experiment, oxalic acid was also studied for regeneration of the AAM. The AAM used in the regeneration experiment adsorbed zinc (15 mg g^{-1}). Three different oxalic acid concentrations and five regeneration times were investigated. Higher concentrations and longer regeneration times increased the regeneration efficiency. The results are presented in Table 9.

In the second adsorption cycle, the same zinc concentration and adsorbent dosage were used. The regeneration time and oxalic acid concentration had a substantial impact on the adsorption efficiency achieved. At an oxalic acid concentration of 0.05 M, the regeneration efficiency was slightly lower than that with concentrations of 0.1 M or 0.2 M. However, a huge difference between the q-values in second adsorption was
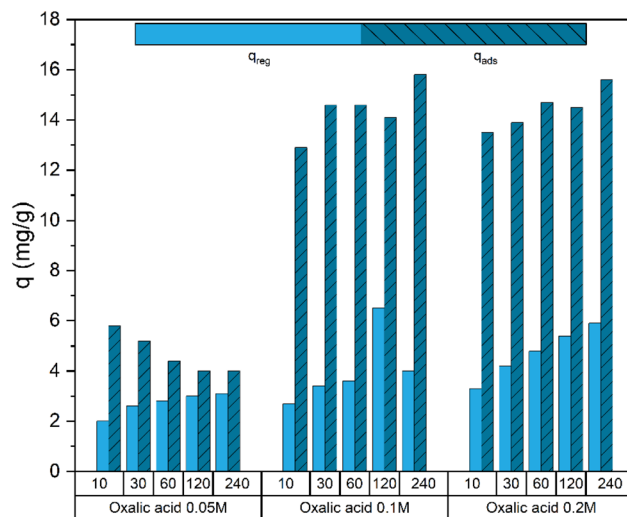

Fig. 11 The effect of the regeneration time (minutes) and oxalic acid concentration on the regeneration and adsorption efficiencies after the first adsorption cycle ($q_{ads} = 15$ mg g^{-1}). The liquid to solid ratio was 10 g L^{-1} and temperature was 25 °C.

detected. The adsorption efficiency was four times greater when using oxalic acid with higher concentrations for regeneration. The adsorption efficiency achieved in the second cycle was close to the value obtained in the first cycle, when regenerated with 0.1 M or 0.2 M oxalic acid. The effects of different regeneration times and regeneration chemical concentrations on the removal efficiency (q_{reg}) and adsorption efficiency in the second cycle (q_{ads}) are illustrated in Fig. 11.

In the literature, regeneration efficiency is usually classified according to how many impurities can be removed from an adsorbent material with the regeneration chemical. However, the removal of impurities is not always the best indicator of regeneration efficiency.[37] Most studies have found that eventually the adsorption capacity for metals decreases after regeneration.[21,46,47] Furthermore, some studies have not investigated the adsorption capacity for the next adsorption cycle at all.[48] The adsorption capacity may decrease because the prewashing chemical affects the surface of the material, including its functional groups. Thus, it is important to investigate surface phenomena and the effect of regeneration on the next adsorption cycle. A significant finding of this study was that the selected regeneration chemical did not have a negative impact

Table 9 Effect of the concentration of oxalic acid as a regeneration agent and time on the regeneration efficiency and second cycle adsorption efficiency with the oxalic acid prewashed AAM

	Regeneration chemical														
	0.05 M oxalic acid					0.1 M oxalic acid					0.2 M oxalic acid				
t_{reg} (min)	10	30	60	120	240	10	30	60	120	240	10	30	60	120	240
1st q_{ads} (mg g^{-1})	15.0	15.0	15.0	15.0	15.0	15.0	15.0	15.0	15.0	15.0	15.0	15.0	15.0	15.0	15.0
1st q_{reg} (mg g^{-1})	2.0	2.6	2.8	3.0	3.1	2.7	3.4	3.6	3.5	4.0	3.3	4.2	4.8	5.4	5.9
2nd q_{ads} (mg g^{-1})	5.8	5.2	4.4	4.0	4.0	12.9	14.6	14.6	14.1	15.8	13.5	13.9	14.7	14.5	15.6

20994 | J. Mater. Chem. A, 2025, **13**, 20984–20997

This journal is © The Royal Society of Chemistry 2025

on the material's surface functionality. The adsorption capacity remained the same in the second adsorption cycle, despite regeneration.

4. Conclusions

The AAM prepared from industrial steel slag side streams was found to be an effective adsorbent. The type of prewashing agent selected had a significant effect on adsorption efficiency achieved. The use of strong (hydrochloric acid and nitric acid) and weak (acetic acid) acids as prewashing agents damaged the material. Oxalic acid as a prewashing agent did not cause material damage. However, the oxalic acid concentration and washing time selected influenced its adsorption efficiency. For AAM, the most promising prewashing concentration and washing time were 0.05 M and 18 h, respectively. Using these prewashing parameters, the adsorption efficiency increased 18 times for zinc, from 0.8 mg g^{-1} to 14.28 mg g^{-1}. Adsorption was optimized *via* an experimental design tool. After optimization, the highest adsorption capacity achieved was 78 mg g^{-1}. As shown by the adsorption and regeneration studies, the regeneration ability of the AAM was good when oxalic acid at concentrations higher than 0.1 M were used. At these concentrations, the efficiency of the adsorbent remained unchanged in subsequent adsorption–regeneration cycles. The AAM was characterized by XRD, XRF, XPS, FESEM-EDS, and DRIFTS. The results showed that washing with oxalic acid affected calcium-containing groups on the surface of the AAM. Based on this and the other surface analyses, the adsorption mechanism is most likely complex formation. From environmental viewpoints, this study convinced that effective material for zinc removal can be produced in a more environmentally friendly way, without harsh acids or huge consumption of pure water. Also, the material showed regenerability, which makes it stand out for the longer usage and zero-waste strategy, key characteristics needed for future materials for water purification. This affects the environment in the long term not only by effective water purification methods but also because of the minimization of steel industry waste by using it as a secondary resource.

Data availability

Any request for the data or additional information should be directed to the corresponding author Hanna Runtti (hanna.runtti@oulu.fi).

Conflicts of interest

There are no conflicts to declare.

Acknowledgements

References

1 M. Procházková, M. Touš, D. Horňák, V. Miklas, M. Vondra and V. Máša, Industrial wastewater in the context of European Union water reuse legislation and goals, *J. Cleaner Prod.*, 2023, **426**, 139037, DOI: **10.1016/j.jclepro.2023.139037**.

2 H. Patel, Batch and continuous fixed bed adsorption of heavy metals removal using activated charcoal from neem (Azadirachta indica) leaf powder, *Sci. Rep.*, 2020, **10**(1), 16895, DOI: **10.1038/s41598-020-72583-6**.

3 S. Bolisetty, M. Peydayesh and R. Mezzenga, Sustainable technologies for water purification from heavy metals: review and analysis, *Chem. Soc. Rev.*, 2019, **48**(2), 463–487, DOI: **10.1039/C8CS00493E**.

4 S. Iftekhar, D. L. Ramasamy, V. Srivastava, M. B. Asif and M. Sillanpää, Understanding the factors affecting the adsorption of Lanthanum using different adsorbents: A critical review, *Chemosphere*, 2018, **204**, 413–430, DOI: **10.1016/J.CHEMOSPHERE.2018.04.053**.

5 H. Hu and K. Xu, Physicochemical technologies for HRPs and risk control, *High-Risk Pollutants in Wastewater*, 2020, pp. 169–207, DOI: **10.1016/B978-0-12-816448-8.00008-3**.

6 C. Shi, X. Wang, S. Zhou, X. Zuo and C. Wang, Mechanism, application, influencing factors and environmental benefit assessment of steel slag in removing pollutants from water: A review, *J. Water Process Eng.*, 2022, **47**, 102666, DOI: **10.1016/J.JWPE.2022.102666**.

7 K.-H. Yang, K.-H. Lee, J.-K. Song and M.-H. Gong, Properties and sustainability of alkali-activated slag foamed concrete, *J. Cleaner Prod.*, 2014, **68**, 226–233, DOI: **10.1016/j.jclepro.2013.12.068**.

8 H. Yi, G. Xu, H. Cheng, J. Wang, Y. Wan and H. Chen, An Overview of Utilization of Steel Slag, *Procedia Environ. Sci.*, 2012, **16**, 791–801, DOI: **10.1016/J.PROENV.2012.10.108**.

9 S. K. Mondal, A. Welz, F. Rezaei, A. Kumar and M. U. Okoronkwo, Structure–Property Relationship of Geopolymers for Aqueous Pb Removal, *ACS Omega*, 2020, **5**(34), 21689–21699, DOI: **10.1021/acsomega.0c02591**.

10 A. T. Ojedokun and O. S. Bello, Sequestering heavy metals from wastewater using cow dung, *Water Resour. Ind.*, 2016, **13**, 7–13, DOI: **10.1016/J.WRI.2016.02.002**.

11 D. Wang, *et al.*, Zinc in soil reflecting the intensive coal mining activities: Evidence from stable zinc isotopes analysis, *Ecotoxicol. Environ. Saf.*, 2022, **239**, 113669, DOI: **10.1016/J.ECOENV.2022.113669**.

12 M. D. Öztel, A. Kuleyin and F. Akbal, Treatment of zinc plating wastewater by combination of electrocoagulation and ultrafiltration process, *Water Sci. Technol.*, 2020, **82**(4), 663–672, DOI: **10.2166/wst.2020.357**.

This journal is © The Royal Society of Chemistry 2025

J. Mater. Chem. A, 2025, **13**, 20984–20997 | **20995**

13 E. I. Ugwu and J. C. Agunwamba, A review on the applicability of activated carbon derived from plant biomass in adsorption of chromium, copper, and zinc from industrial wastewater, *Environ. Monit. Assess.*, 2020, **192**(4), 240, DOI: **10.1007/s10661-020-8162-0**.

14 *Atlas of Eh-pH diagrams Intercomparison of thermodynamic databases*, 2005.

15 M. P. Christophliemk, *et al.*, Preparation and characterization of porous and stable sodium- and potassium-based alkali activated material (AAM), *Appl. Clay Sci.*, 2022, **230**, 106697, DOI: **10.1016/J.CLAY.2022.106697**.

16 M. Manninen, T. Kangas, T. Hu, T. Varila, U. Lassi and H. Runtti, Zn(II) Removal from Wastewater by an Alkali-Activated Material Prepared from Steel Industry Slags: Optimization and Modelling of a Fixed-Bed Process, *Environ. Technol.*, 2023, 1–73, DOI: **10.1080/09593330.2023.2177565**.

17 G. Bumanis, R. M. Novais, J. Carvalheiras, D. Bajare and J. A. Labrincha, Metals removal from aqueous solutions by tailored porous waste-based granulated alkali-activated materials, *Appl. Clay Sci.*, 2019, **179**, 105147, DOI: **10.1016/J.CLAY.2019.105147**.

18 C. Sarkar, J. K. Basu and A. N. Samanta, Synthesis of mesoporous geopolymeric powder from LD slag as superior adsorbent for Zinc (II) removal, *Adv. Powder Technol.*, 2018, **29**(5), 1142–1152, DOI: **10.1016/j.apt.2018.02.005**.

19 M. Lu, *et al.*, Potentiality of the porous geopolymer sphere in adsorption of Pb (II) from aqueous solutions: Behaviors and mechanisms, *Ceram. Int.*, 2023, **49**(1), 698–706, DOI: **10.1016/j.ceramint.2022.09.040**.

20 S. Onutai, T. Kobayashi, P. Thavorniti and S. Jiemsirilers, Porous fly ash-based geopolymer composite fiber as an adsorbent for removal of heavy metal ions from wastewater, *Mater. Lett.*, 2019, **236**, 30–33, DOI: **10.1016/J.MATLET.2018.10.035**.

21 E. Sundhararasu, *et al.*, Alkali-Activated Adsorbents from Slags: Column Adsorption and Regeneration Study for Nickel(II) Removal, *ChemEngineering*, 2021, **5**(1), 13, DOI: **10.3390/chemengineering5010013**.

22 J. Tang, *et al.*, Optimization of coal fly ash-based porous geopolymer synthesis and application for zinc removal from water, *Ceram. Int.*, 2023, **49**(4), 5828–5833, DOI: **10.1016/j.ceramint.2022.10.028**.

23 K. Sun, H. A. Ali, W. Ji, J. Ban and C. S. Poon, Utilization of contaminated air pollution control residues generated from sewage sludge incinerator for the preparation of alkali-activated materials, *Resour., Conserv. Recycl.*, 2023, **188**, 106665, DOI: **10.1016/J.RESCONREC.2022.106665**.

24 E. Repo, J. K. Warchoł, L. J. Westholm and M. Sillanpää, Steel slag as a low-cost sorbent for metal removal in the presence of chelating agents, *J. Ind. Eng. Chem.*, 2015, **27**, 115–125, DOI: **10.1016/j.jiec.2014.12.025**.

25 İ. Kara, D. Yilmazer and S. T. Akar, Metakaolin based geopolymer as an effective adsorbent for adsorption of zinc(II) and nickel(II) ions from aqueous solutions, *Appl. Clay Sci.*, 2017, **139**, 54–63, DOI: **10.1016/j.clay.2017.01.008**.

26 Y. Liao, W. Ge, M. Liu, W. Bi, C. Jin and D. D. Y. Chen, Eco-friendly regeneration of lignin with acidic deep eutectic solvent for adsorption of pollutant dyes for water cleanup, *Int. J. Biol. Macromol.*, 2024, **260**, 129677, DOI: **10.1016/J.IJBIOMAC.2024.129677**.

27 H. Aguiar, J. Serra, P. González and B. León, Structural study of sol–gel silicate glasses by IR and Raman spectroscopies, *J. Non-Cryst. Solids*, 2009, **355**(8), 475–480, DOI: **10.1016/J.JNONCRYSOL.2009.01.010**.

28 W. Mao, H. Ma and B. Wang, A clean method for solvent-free nitration of toluene over sulfated titania promoted by ceria catalysts, *J. Hazard. Mater.*, 2009, **167**(1–3), 707–712, DOI: **10.1016/J.JHAZMAT.2009.01.045**.

29 W. Mozgawa and J. Deja, Spectroscopic studies of alkaline activated slag geopolymers, *J. Mol. Struct.*, 2009, **924–926**(C), 434–441, DOI: **10.1016/J.MOLSTRUC.2008.12.026**.

30 W. K. W. Lee and J. S. J. van Deventer, Use of Infrared Spectroscopy to Study Geopolymerization of Heterogeneous Amorphous Aluminosilicates, *Langmuir*, 2003, **19**(21), 8726–8734, DOI: **10.1021/la026127e**.

31 J. B. Lambert, H. F. Shurvell, D. A. Lightner and R. G. Cooks, *Organic Structural Spectroscopy*, Prentice-Hall, Upper Saddle River (N.J.), 1998.

32 P. Lalitha, S. Arumugam, A. Sinthiya, C. Nivetha and M. Muthuselvam, Oxalic acid incorporated acetamide single crystal growth dynamics, characterization, NLO and antimicrobial activities via shock wave treatment, *Results Chem.*, 2023, **5**, 100790, DOI: **10.1016/J.RECHEM.2023.100790**.

33 V. F. F. Barbosa, K. J. D. MacKenzie and C. Thaumaturgo, Synthesis and characterisation of materials based on inorganic polymers of alumina and silica: sodium polysialate polymers, *Int. J. Inorg. Mater.*, 2000, **2**(4), 309–317, DOI: **10.1016/S1466-6049(00)00041-6**.

34 M. L. Granizo, S. Alonso, M. T. Blanco-Varela and A. Palomo, Alkaline Activation of Metakaolin: Effect of Calcium Hydroxide in the Products of Reaction, *J. Am. Ceram. Soc.*, 2002, **85**(1), 225–231, DOI: **10.1111/j.1151-2916.2002.tb00070.x**.

35 Z. Zhang, Y. Zhong, W. Zhang, P. Zhao, H. Li and X. Liu, The Preparation and Application in Adsorptive Removal Hazardous Materials of MOF-Derived Materials, *J. Inorg. Organomet. Polym. Mater.*, 2023, **33**, 1–25, DOI: **10.1007/s10904-023-02784-9**.

36 M. Ponnuchamy, *et al.*, Sustainable adsorbents for the removal of pesticides from water: a review, *Environ. Chem. Lett.*, 2021, **19**, 2425–2463, DOI: **10.1007/s10311-021-01183-1**.

37 P. Arokiasamy, *et al.*, Diverse material based geopolymer towards heavy metals removal: a review, *J. Mater. Res. Technol.*, 2023, **22**, 126–156, DOI: **10.1016/J.JMRT.2022.11.100**.

38 J. A. Gómez del Río, P. J. Morando and D. S. Cicerone, Natural materials for treatment of industrial effluents: comparative study of the retention of Cd, Zn and Co by calcite and hydroxyapatite. Part I: batch experiments, *J. Environ. Manage.*, 2004, **71**(2), 169–177, DOI: **10.1016/j.jenvman.2004.02.004**.

20996 | *J. Mater. Chem. A*, 2025, **13**, 20984–20997

This journal is © The Royal Society of Chemistry 2025

39 R. M. Novais, L. H. Buruberri, M. P. Seabra and J. A. Labrincha, Novel porous fly-ash containing geopolymer monoliths for lead adsorption from wastewaters, *J. Hazard. Mater.*, 2016, **318**, 631–640, DOI: **10.1016/j.jhazmat.2016.07.059**.

40 K. K. Al-Zboon, B. M. Al-smadi and S. Al-Khawaldh, Natural Volcanic Tuff-Based Geopolymer for Zn Removal: Adsorption Isotherm, Kinetic, and Thermodynamic Study, *Water, Air, Soil Pollut.*, 2016, **227**(7), 248, DOI: **10.1007/s11270-016-2937-5**.

41 A. P. F. Caetano, *et al.*, Unravelling the Affinity of Alkali-Activated Fly Ash Cubic Foams towards Heavy Metals Sorption, *Materials*, 2022, **15**(4), 1453, DOI: **10.3390/ma15041453**.

42 S. Andrejkovičová, *et al.*, The effect of natural zeolite on microstructure, mechanical and heavy metals adsorption properties of metakaolin based geopolymers, *Appl. Clay Sci.*, 2016, **126**, 141–152, DOI: **10.1016/j.clay.2016.03.009**.

43 D. Lita, N. Suprihanto, D. Enri, T. M. Kadja Grandprix and R. M. Rino, Preparation of alkali-activated fly ash-based geopolymer and their application in the adsorption of copper (II) and zinc (II) ions, *MATEC Web Conf.*, 2019, **276**, 6012, DOI: **10.1051/matecconf/201927606012**.

44 S. K. Mondal, *et al.*, Examining the Effect of a Chitosan Biopolymer on Alkali-Activated Inorganic Material for Aqueous Pb(II) and Zn(II) Sorption, *Langmuir*, 2022, **38**(3), 903–913, DOI: **10.1021/acs.langmuir.1c01829**.

45 A. Purbasar, D. Ariyanti, S. Sumardiono, M. A. Shofa and R. P. Manullang, Comparison of Alkali Modified Fly Ash and Alkali Activated Fly Ash as Zn(II) Ions Adsorbent from Aqueous Solution, *Sci. Sinter.*, 2022, **54**(1), 1–10, DOI: **10.2298/SOS2201049P**.

46 N. P. F. Gonçalves, E. F. da Silva, L. A. C. Tarelho, J. A. Labrincha and R. M. Novais, Simultaneous removal of multiple metal(loid)s and neutralization of acid mine drainage using 3D-printed bauxite-containing geopolymers, *J. Hazard. Mater.*, 2024, **462**, 132718, DOI: **10.1016/j.jhazmat.2023.132718**.

47 Z. Yu, S. Weifeng and P. Ding, Mesoporous geopolymer for improved adsorption and immobilization of copper ions, *Desalin. Water Treat.*, 2020, **201**, 278–288, DOI: **10.5004/dwt.2020.25926**.

48 S. M. Abdelbasir and M. A. A. Khalek, From waste to waste: iron blast furnace slag for heavy metal ions removal from aqueous system, *Environ. Sci. Pollut. Res.*, 2022, **29**(38), 57964–57979, DOI: **10.1007/s11356-022-19834-3**.

This journal is © The Royal Society of Chemistry 2025

J. Mater. Chem. A, 2025, **13**, 20984–20997 | **20997**